Materials Science and Engineering C 59 (2016) 901–908

Contents lists available at ScienceDirect

Materials Science and Engineering C

journal homepage: www.elsevier.com/locate/msec

Improving bone cement toughness and contrast agent confinement by using acrylic branched polymers

Maria H. Lissarrague [a,b], Mirta L. Fascio [a], Silvia Goyanes [b,*], Norma B. D'Accorso [a,*]

[a] CIHIDECAR-CONICET; Departamento de Química Orgánica, FCEyN — UBA, Ciudad Universitaria 1428, Ciudad Autónoma de Buenos Aires, Argentina
[b] IFIBA — CONICET; LP&MC, Departamento de Física, FCEyN — UBA, Ciudad Universitaria 1428, Ciudad Autónoma de Buenos Aires, Argentina

ARTICLE INFO

Article history:
Received 15 July 2015
Received in revised form 6 October 2015
Accepted 29 October 2015
Available online 30 October 2015

Keywords:
Branched polymer
Poly(methyl methacrylate)
Natural rubber
Polyisoprene
Barium sulphate nanoparticles

ABSTRACT

A new biomedical material to be used as part of acrylic bone cement formulations is described. This new material is tough, its Young's Modulus is similar to the one of poly (methylmethacrylate) and the contrast agent, usually employed in acrylic bone cements, is homogeneously distributed among the polymeric matrix. Additionally, its wear coefficient is 66% lower than the one measured in poly(methyl methacrylate). The developed material is a branched polymer with polyisoprene backbone and poly(methyl methacrylate) side chains, which are capable of retaining barium sulphate nanoparticles thus avoiding their aggregation. The grafting reaction was carried out in presence of the nanoparticles, using methyl methacrylate as solvent. From the ^{1}H-NMR spectra it was possible to determine the average number of MMA units per unit of isoprene (3.75:1). The ability to retain nanoparticles (about 8 wt.%), attributed to their interaction with the polymer branches, was determined by thermogravimetric analysis and confirmed by FTIR and microscopy techniques. By SEM microscopy it was also possible to determine the homogeneous spatial distribution of the barium sulphate nanoparticles along the polymer matrix.

1. Introduction

Nowadays, poly(methyl methacrylate) (PMMA) and its derivatives are widely used in the biomedical field due to their biocompatibility, biostability and easy manipulation [1]. Indeed, it is one of the main components of acrylic bone cements which are of major use in orthopaedics [2]. Acrylic bone cements are both used in order to anchor prostheses (arthroplasty) and to augment fractured vertebra (vertebroplasty and kyphoplasty). The mechanical behaviour of the acrylic bone cement plays a major role in the long term success of the surgical procedure.

In recent years, many researchers have focused their investigations in the biomechanics of repaired vertebrae [3]. These studies suggest that this cement injection may cause an increase in the failure load and stiffness of the fractured vertebra which might lead to a redistribution of loads through the adjacent vertebrae and thus increase the risk of adjacent vertebral fractures [4]. In this sense, PMMA is a brittle material with limited ability to absorb energy and transform it into plastic deformation. On the contrary, human bone tissue is capable of deforming plastically [5].

Additionally, vertebroplasty and kyphoplasty require fluoroscopic or x-ray imaging control of the surgical procedure in order to avoid extravasation. As PMMA is a radiolucent material, it requires the addition of a contrast agent, e.g. barium sulphate particles. These composite materials have several drawbacks related to the inhomogeneous distribution of the particles within the PMMA matrix which may lead to a deficient fluoroscopic control of the procedure. The development of a composite material with a high weight ratio of the filler relative to the polymer matrix is not an alternative to overcome this issue as it will possibly affect negatively the mechanical performance of the acrylic bone cement [6,7], as agglomerates of $BaSO_4$ could worsen the already poor toughness of PMMA [1].

The modification of the polymeric matrix seems the most suitable alternative may be a suitable alternative to in order to develop new acrylic bone cement with improved mechanical behaviour overcome these issues [8].

The incorporation of an elastomeric polymer as polyisoprene (PI) in the bulk of a thermoplastic brittle polymer, in this case PMMA, might improve its toughness. However, these two phases are immiscible and no improvement is achieved. A similar behaviour was observed in blends of polystyrene (PS) and natural rubber (NR) [9,10]. To overcome this issue it was suggested the use of natural rubber grafted with PS (NR-*g*-PS) as compatibilizer. Due to the presence of the PS branches, the miscibility between the PS matrix and the NR-*g*-PS increased and an enhancement in toughness of PS was observed. This same procedure is proposed in order to obtain a tougher PMMA-based polymeric matrix [11,12].

´Grafting´ is a methodology where monomers are covalently bonded to a polymer chain backbone [13]. The most simple methodology to obtain polyisoprene grafted poly(methyl metacrylate) (PI-*g*-PMMA) is the bulk polymerization mechanism where the MMA is used as the solvent

* Corresponding authors.
E-mail addresses: goyanes@df.uba.ar (S. Goyanes), norma@qo.fcen.uba.ar (N.B. D'Accorso).

http://dx.doi.org/10.1016/j.msec.2015.10.097
0928-4931/

[14]. Other methodologies include: the emulsion polymerization where a natural rubber latex is employed [15]; a grafting methodology involving the atom transfer radical polymerization where the PI was transformed into macro initiator using two-step chemical modification described by Vayachuta et al. [16]; and finally the photopolymerization of methyl methacrylate (MMA) initiated by *N*,*N*-diethyldithiocarbamate described by Derouet et al., which was synthesized by groups created beforehand in side positions on the PI chains [17].

The grafting technique has also proven to be a successful methodology for embed and/or confine metal and semiconducting nanoparticles [18]. In this sense, Amhad et al. [19,20] described the synthesis of polymeric electrolyte films, prepared using poly(methyl methacrylate) grafted natural rubber (MG49) in presence of both lithium salts and mixtures of lithium salts and stannum oxide. These results points out the usefulness of the grafting technique in order to entrap nanoparticles. Additionally, it has been proven that PMMA interacts with SiO_2 nanoparticles in such a way that polymer chains are immobilized at the interface, even though these interactions are not covalent bonds [21].

To the best of our knowledge, this strategy has not been employed to develop a tougher polymeric matrix capable of confining the contrast agent, to be used as part of acrylic bone cement formulations.

The aim of this work is to obtain a PMMA based material but with enhanced toughness and higher wear resistance which must also be capable of entrapping the contrast agent and confining it homogeneously. In this sense, a graft polymer with PI backbone and short PMMA side chains homogeneously distributed along the principal chain was synthesized. The grafting reaction was carried out in presence of the $BaSO_4$ nanoparticles and using MMA as solvent.

The grafting efficacy was evaluated by Nuclear Magnetic Resonance spectroscopy (NMR) and confirmed by microanalysis and infrared spectroscopy (FT-IR). The thermal behaviour of the grafted polymers was investigated using differential scanning calorimetry (DSC) and thermogravimetric analysis (TGA). TGA is also employed to determine the $BaSO_4$ nanoparticles content. Additionally, the morphology of the resulting material was observed by scanning electron microscopy (SEM). The Young's modulus, stress and strain at break and tensile toughness of the obtained materials were evaluated and compared with the values obtained for ungrafted PI. Finally, the wear coefficient of both grafted materials was measured.

2. Experimental

2.1. Materials

Polyisoprene (Mw 525,518 g/mol; Mn 365,426 g/mol; P 1, 44) was provided by FATE SAICI. It was purified by dissolution in petroleum ether and precipitation with methanol, and finally dried under vacuum at room temperature. Barium sulphate nanoparticles Blanc Fixe XR Series were provided by Sachtleben Chemie GmbH. Dichloromethane, acetone, and benzoyl peroxide (BPO; 75%) were purchased from Aldrich and used as received. MMA was previously purified using a column packed with basic Al_2O_3. PMMA employed for comparison purposes was obtained from commercial high viscosity acrylic bone cement, usually employed in vertebroplasty. As this bone cement is a mixture of PMMA and $BaSO_4$, it was necessary to separate previously the polymer from the contrast agent. This PMMA was characterized through Size Exclusion Chromatography. Its molecular weight distribution was 97% Mw 152,707 g/mol, Mn 100,121 g/mol; and 3% Mw 979,455 g/mol, Mn 976,502 g/mol.

2.2. Preparation of PI and PMMA graft copolymer

The polymerization was conducted in a test tube under nitrogen atmosphere, where 200 mg of purified PI are dissolved in 1 mL of MMA at a temperature of 70 °C until a gel is formed. Afterwards, 50 mg of BPO are dissolved in 0.2 mL of MMA and then added to the reaction mixture. The reaction is left at 70 °C for 4 h. The obtained polymer is left in contact with acetone for 36 h to remove traces of PMMA homopolymer. Afterwards, it was filtered and washed three times with fresh portions of hot acetone. The same procedure was repeated with petroleum ether in order to remove traces of PI. Finally, the PI-*g*-PMMA was dissolved in dichloromethane, precipitated with methanol and then dried under vacuum.

A similar procedure to the one described above was followed in order to obtain the grafted material with $BaSO_4$ nanoparticles. In this case, $BaSO_4$ nanoparticles (20% *w*/*w* respect to PI) were added after the gel was formed.

Fig. 1 shows the synthetic scheme to obtain PI-*g*-PMMA or PI-*g*-PMMA/NPs when the $BaSO_4$ nanoparticles are present during the reaction.

2.3. Film preparation

For film preparation, 140 mg of PI-*g*-PMMA or PI-*g*-PMMA/NPs were dissolved in 15 mL of dichloromethane, casted in a glass container, dried in air for 24 h and then dried under vacuum at 60 °C for 5 days. The complete elimination of dichloromethane was evaluated by ^{1}H NMR and TGA. The thickness of the obtained films was of 25 ± 1 μm. The PI film was prepared using petroleum ether instead of dichloromethane.

2.4. Characterization

2.4.1. Nuclear Magnetic Resonance (NMR)

^{1}H and ^{13}C NMR and 2D HSQC (Heteronuclear Single Quantum Coherence) spectra were recorded on a Bruker AMX-500 spectrometer operating at 500 and 125 MHz for ^{1}H and ^{13}C NMR respectively. All spectra were performed using $CDCl_3$ as solvent and tetramethylsilane (TMS) as internal standard.

2.4.2. Elemental analysis

The elemental analysis was performed on an Exeter Analytical CE-440 Elemental Analyser.

2.4.3. Fourier transform infrared spectroscopy (FT-IR)

Fourier transform infrared (FT-IR) spectra were measured with a Nicolet 510 P spectrometer coupled with an attenuated total reflectance (ATR) accessory. The spectra recorded are an average of 32 scans.

2.4.4. Thermogravimetric analysis (TGA)

Thermogravimetric measurements were made on a SHIMADZU DTG-60, under dry nitrogen atmosphere (20 mL/min). Between 3 and 5 mg of the samples were placed in aluminium pans inside the thermogravimetric balance. Samples were heated to 500 °C at a heating rate a rate of 10 °C min^{-1}.

2.4.5. Differential scanning calorimetry (DSC)

Calorimetric measurements were made on a TA Q20 differential scanning calorimeter under a dry nitrogen atmosphere. Indium standard was used for calibration. Samples of 5–10 mg were placed in the DSC pan. Samples were first heated to 150 °C at a rate of 10 °C min^{-1}, then cooled down to −80 °C, held at this temperature for 10 min, and again heated to 150 °C at 10 °C min^{-1}. All T_g values were taken as the midpoint of the transition in the second heating scan.

2.4.6. Field emission scanning electron microscopy (FE-SEM)

Micrographs of the fracture surface of films of the synthesized materials were obtained using a Field Emission Scanning Electron

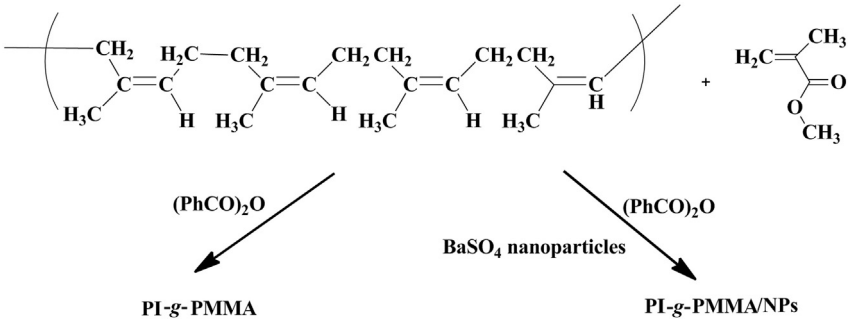

Fig. 1. Synthetic pathway proposed to obtain the grafted products.

Microscope Zeiss Leo 982 GEMINI. Samples were prepared via cryogenic fracture of films, which were then sputtered with gold.

2.4.7. Quasi-static mechanical testing

The tensile stress–strain behaviour was evaluated using a DMTA IV Rheometric Scientific Inc., in a Strain Rate Test, where the strain rate was 10^{-4} seg^{-1}. The experiment was performed till rupture. The sample shape was designed according to ASTM D 4065.

Five samples of each material were tested and the reported results are the average value of the data obtained for each sample and the standard deviation.

2.4.8. Ball cratering micro-scale wear test

The ball cratering micro-scale wear test was performed using a Calotest device [22]. In order to produce the desired crater, a stainless steel ball of 12.68 mm diameter and 16.30 g was employed at a rolling speed of 245 RPM.

3. Results and discussion

3.1. Structural analysis

3.1.1. NMR

In order to characterize the new material (PI-*g*-PMMA) via NMR, the ^{1}H NMR spectra both homopolymers, PI and PMMA, were performed.

The ^{1}H NMR spectrum of PI shows the olefin protons as a broad singlet at δ 5.12 ppm, the methylene protons at δ 2.10 ppm and the methyl proton at δ 1.68 ppm as it was previously reported [23,24].

The ^{1}H NMR spectrum of PMMA shows different signals corresponding to methoxy protons at δ 3.60 ppm. The signals attributed to methyl protons appear around δ 0.90 and 1.20 ppm. The signals between δ 1.75 and 2.01 ppm can be attributed to methylene protons. As PMMA shows two different molecular weight distributions, its polydispersity may explain the existence of different signals corresponding to the same chemical group. As an example, it is possible to observe several signals corresponding to methyl protons and different signals for methoxy protons.

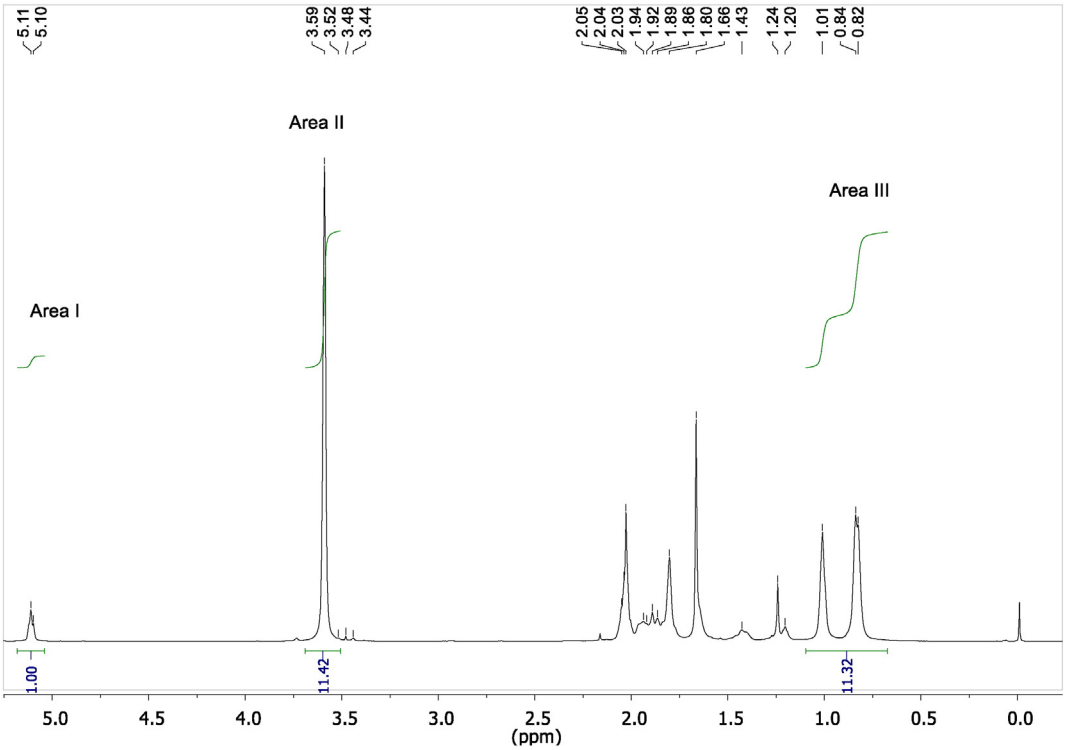

Fig. 2. ^{1}H NMR spectra and pick area of PI-*g*-PMMA: isoprene vinyl protons (Area I), PMMA methoxy protons (Area II) and PMMA methyl protons (Area III).

The ^{1}H NMR spectrum of PI-*g*-PMMA (Fig. 2) showed the signals corresponding to PI as well as the signal corresponding to the different protons of the PMMA; however it is important to notice that the integration between the different signals of PI and PMMA are not the same of those of individual spectra. This observation confirmed the grafting reaction. Similar results were observed by Kochthongrasamee et al. [24] while studying the effect of three types of redox initiators on the grafting extent of MMA on natural rubber.

Based on the assumption that the most stable radicals formed on PI during the grafting reaction are the allylic-type radicals, particularly the ones belonging to the methylene protons; it is possible to consider that the vinyl protons of PI which appear at δ 5.11 ppm (Fig. 2 — Area I) are not modified during the polymerization. Similarly, the signals of PMMA at δ 3.59 ppm (PMMA methoxy signals, Fig. 2 — Area II) or 1.01, 0.84 and 0.82 ppm (PMMA methyl protons, Fig. 2 — Area III) are not modified during reaction. It is therefore possible to estimate the MMA units per isoprene unit incorporated during the grafting reaction. The peak areas of ^{1}H NMR spectrum signals of the PI-*g*-PMMA sample are shown in Fig. 2. In this sense, the peak area of the unsaturated methyne protons (olefin proton, Area I) is assigned as the unitary value and the areas corresponding of the methoxy protons (Area II) and the methyl protons (Area III) of PMMA, corresponding to three protons, are 11.33 and 11.19, respectively. Having in mind these values it is possible to estimate that on average 3.75 units of MMA are incorporated per unit of isoprene.

3.1.2. Elemental analysis

The elemental analysis of the PI-*g*-PMMA was carried out in order to confirm the relationship between MMA and isoprene units obtained from the analysis of the ^{1}H NMR spectrum.

The material composition obtained by Elemental Analysis was: C: 63.8% and H: 8.3%. It is very interesting to notice that if the theoretical material composition is calculated taking into account the average relationship obtained from the ^{1}H NMR data (3.75 MMA: 1 isoprene), the theoretical values would be: C: 64.2% and H: 8.6%. The difference between theoretical and experimental data is lower than 0.5%, thus confirming the average number of MMA units per isoprene unit, obtained by RMN data.

3.1.3. SEC

From the size exclusion chromatography analysis of PI-*g*-PMMA and pure PI it was possible to identify different molecular weight profiles.

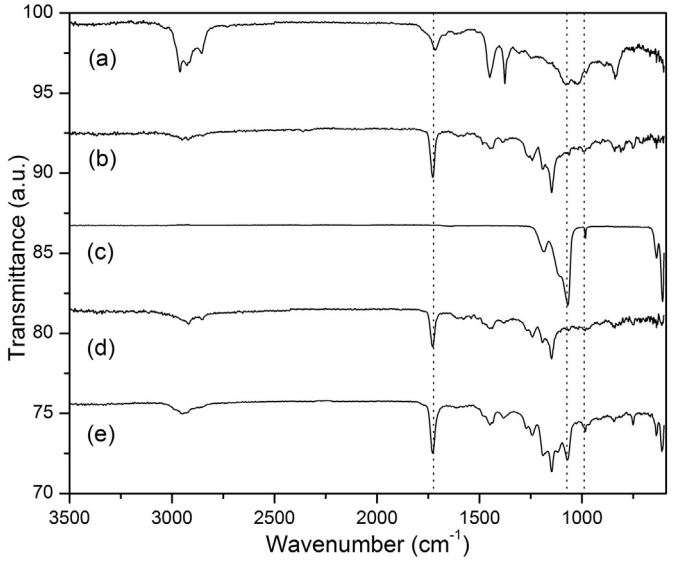

Fig. 3. FT-IR spectra of (a) PI, (b) PMMA, (c) $BaSO_4$ NPs, (d) PI-*g*-PMMA and (e) PI-*g*-PMMA/NPs.

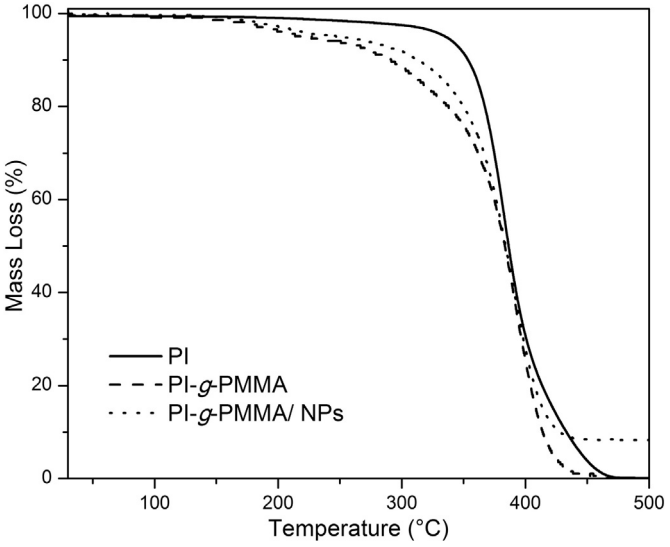

Fig. 4. Termogravimetric curves of PI, PI-*g*-PMMA and PI-*g*-PMMA/NPs.

Due to the fact that the hydrodynamic volume of grafted polymers is very different to the one associated with linear polymers having the same molecular weight, it is important to remark that it is not possible to determine the molecular weight of PI-*g*-PMMA using this methodology as the polymeric standards employed for calibration are linear. Any result would not be representative. However, D. Hall-Edgefield et al. [25] employed this methodology to evidence the formation of their molecular brushes, which are also composed of a natural polymer backbone and synthetic polymer side chains, by evaluating the evolution of the molecular weight profile.

3.1.4. FT-IR

In order to verify the grafting reaction as well as the entrapment of barium sulphate nanoparticles due to the polymeric branches, the FT-IR spectra of PI, PMMA, $BaSO_4$ nanoparticles, PI-*g*-PMMA and PI-*g*-PMMA/NPs were recorded (Fig. 3).

FT-IR spectrum of PI (Fig. 3 a) shows signals at 2919, 1470 and 719 cm^{-1} corresponding to the characteristic absorption bands of methylene groups and signals at 1664 and 1644 cm^{-1} belonging to the C = C stretching [26].

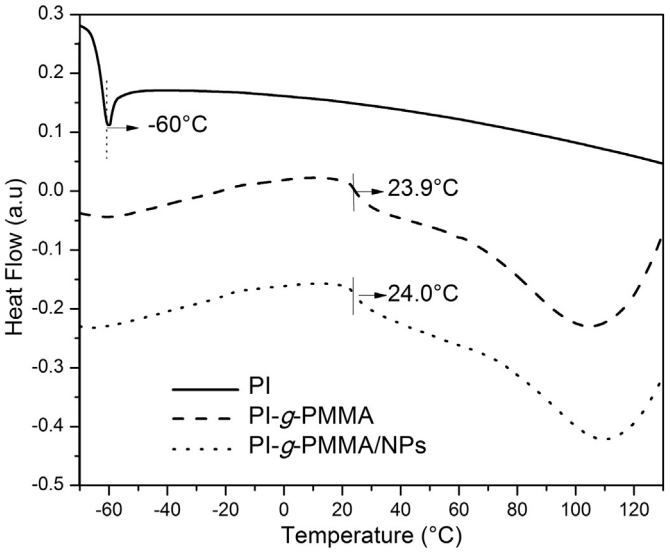

Fig. 5. DSC scans of PI, PI-*g*-PMMA and PI-*g*-PMMA/NPs.

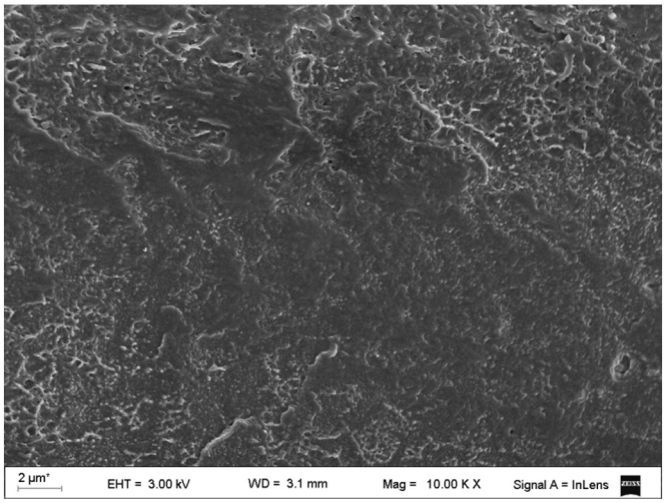

Fig. 6. SEM micrograph of cryogenic fracture surface of PI-*g*-PMMA.

From the analysis of the FTIR spectrum of PMMA (Fig. 3 b) it is possible to observe bands at 2983, 1436 and 1381 cm^{-1} corresponding to the methyl groups and a signal at 1720 cm^{-1} associated with the carbonyl group. In the $BaSO_4$ nanoparticles FITR spectrum (Fig. 3 c) it is possible to observe signals at 1173, 1110 cm^{-1} and the shoulder at 982 cm^{-1} corresponding to the symmetrical vibration of SO_4^{2-}. The signals observed at 633 and 610 cm^{-1} are assigned to the out-of-plane bending vibration of the SO_4^{2-} [27,28].

It is important to notice that the spectrum of PI-*g*-PMMA/NPs (Fig. 3 e) showed both the signals of the FTIR spectrum of PI-*g*-PMMA and the characteristic signal of $BaSO_4$ nanoparticles (1173, 1110 cm^{-1} and 982 cm^{-1}). This allows us to confirm the incorporation of the nanoparticles during the grafting reaction.

3.2. Thermal behaviour

3.2.1. TGA

In order to evaluate the ability of the grafted material to retain $BaSO_4$ nanoparticles the thermogravimetric analysis were performed.

The TGA analysis (Fig. 4) showed a first degradation step in both grafted materials (PI-*g*-PMMA and PI-*g*-PMMA/NPs) at 170 °C, which is not observed on PI, but is in agreement with the mechanisms proposed for the PMMA degradation. L. E. Manring et al. [29,30] reported that the unsaturated ends of PMMA, resulting from termination by disproportionation, were responsible of the two weight loss stages reported around 180 and 270 °C and a random scission degradation of PMMA is the responsible of the degradation step that occurs around 350–400 °C. Although the second degradation step observed in the grafted materials exhibit a similar behaviour to PI, PI-*g*-PMMA degrades at lower temperatures than PI.

In addition, it was observed that the barium sulphate nanoparticles content of PI-*g*-PMMA/NPs was 8 wt.% where the curve reaches a plateau.

3.2.2. DSC

The DSC thermograms of PI, PI-*g*-PMMA and PI-*g*-PMMA/NPs are shown in Fig. 5. It is important to notice that PI has its glass transition temperature (T_g) at −60 °C while in PI-*g*-PMMA and PI-*g*-PMMA/NPs it is 23.9 °C and 24 °C, respectively. Taking into consideration that only one T_g is observed in both grafted materials, it can be concluded that no homopolymer (PI or PMMA) is left after being washed with acetone

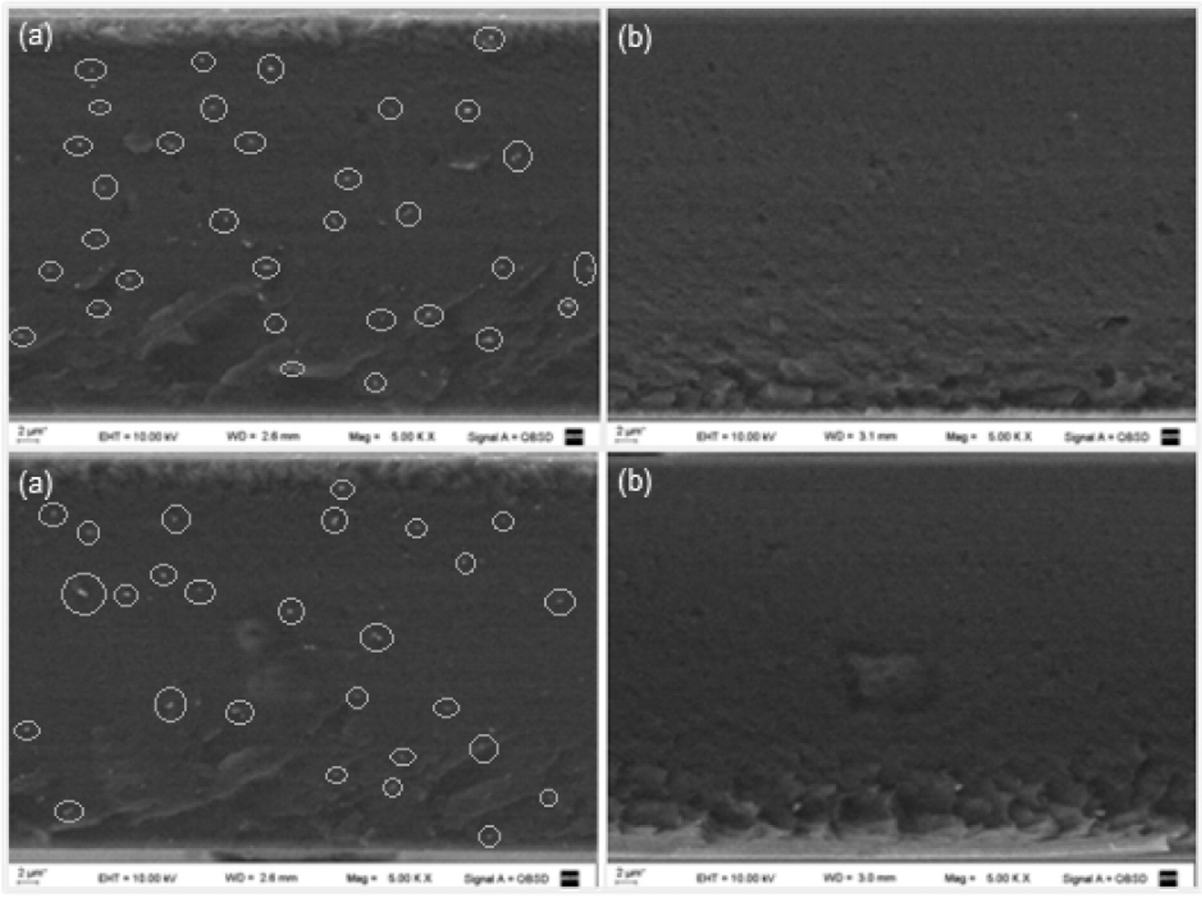

Fig. 7. SEM micrographs using a QBSD detector of the cryogenic fracture surface of both (a) PI-*g*-PMMA/NPs and (b) PI-*g*-PMMA (right).

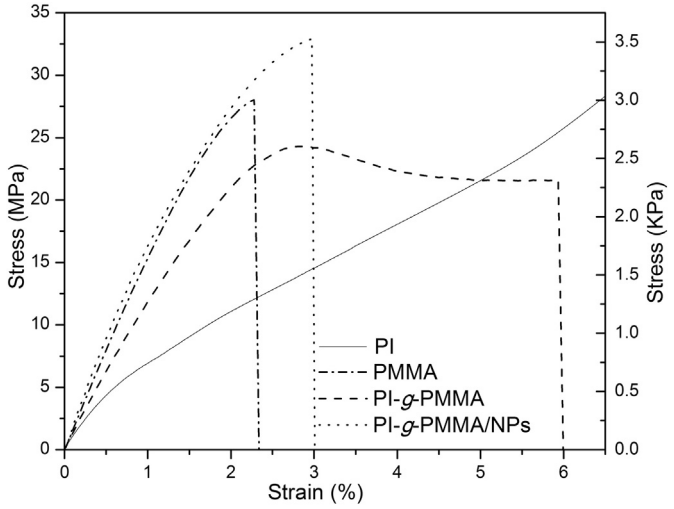

Fig. 8. Stress–strain curves obtained for PI, PMMA, PI-*g*-PMMA and PI-*g*-PMMA/NPs.

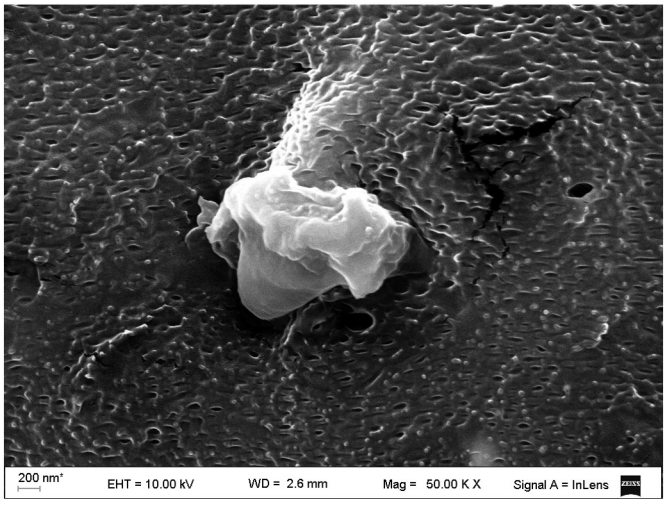

Fig. 9. Nanoparticle adherence in the PI-*g*-PMMA matrix.

and petroleum ether. The increase in both T_g values can be attributed to the rigidization of the PI backbone due to PMMA chains grafted onto it. It is noteworthy that after the grafting reaction is carried out a new material is obtained, with increased rigidity compared to the original one. Taking into consideration that PMMA shows higher rigidity than PI, a higher T_g value is expected in both grafted materials as chain mobility is lower than the one expected for elastomers. Due to the presence of $BaSO_4$ nanoparticles a higher T_g value would be expected in PI-*g*-PMMA/NPs as a consequence of steric effects [31]. However, an increase in the free volume also related to the incorporation of these nanoparticles has the opposite effect. As no difference is observed between the both T_g values, it is not possible to determine whether both effects are taking place, hence cancelling one another, or if none of them are actually affecting noticeably the system.

3.3. Morphology studies

The morphology of the cryogenic fractured surface of PI-*g*-PMMA was analysed through FE-SEM studies, as shown in Fig. 6. In it, it is possible to observe that in its majority the cryogenic fracture surface shows a rough profile thus indicating the heterogenic nature of this branched polymer. It is noteworthy that the analysis of the cryogenic fracture surface is not the analysis of the surface of the sample but the study of a plane perpendicular to the surface of the sample.

Fig. 7a and b show SEM micrographs using a Quadrant Back-Scattering Detector (QBSD) of the cryogenic fracture surface of both grafted materials, with and without nanoparticles. As back scattered electron signals are strongly related with the atomic number (Z) of the sample, QSBD gives rise to SEM micrographs which allows the identification of the $BaSO_4$ nanoparticles within the polymer matrix. Additionally it is possible to identify a homogeneous distribution of the nanoparticles in the matrix.

3.4. Mechanical properties

The mechanical behaviour of PI, PMMA, PI-*g*-PMMA and PI-*g*-PMMA/NPs was studied through quasi-static tensile tests. In this sense, Fig. 8 shows the obtained stress–strain curves for PI, PMMA, PI-*g*-PMMA and PI-*g*-PMMA/NPs; and Table 1 reports the values of Young's modulus, stress at break and tensile toughness for PMMA and both grafted materials. The tensile toughness is defined as the area under the stress–strain curve [32]. This area represents the elastoplastic energy per unit volume absorbed until fracture. Finally, the Young's Modulus of PI is also reported.

The stress–strain curve of PI-*g*-PMMA is consistent with the neck formation observed in the samples studied during the tensile tests, as it indicates the existence of deformation past the yield stress. This ductile behaviour is in agreement with what is observed in thermoplastic materials tested near their T_g. On the contrary, PI-*g*-PMMA/NPs shows fragile failure, a similar behaviour to the one expected in PMMA. Even though the deformation of both grafted materials involves more elastoplastic energy per unit volume than that of commercial PMMA, this parameter varies from PI-*g*-PMMA to PI-*g*-PMMA/NPs. The observed difference may be due to mechanical failure throw crack propagation as a consequence of the presence of the NPs, thus rendering the material more fragile. Although most $BaSO_4$ nanoparticles are adhered to the polymer matrix, there are weak linking zones as can be seen in the micrograph shown in Fig. 9. However, the addition of $BaSO_4$ nanoparticles leads to an enhancement in the stress at break.

Both materials show a very different behaviour to the one observed in PI, which exhibit the characteristic stress–strain curve of an elastomer. It is worth noticing that the values of stress at break for both grafted materials are higher than the one obtained for PI, thus indicating a high concentration of PMMA. The rigidization of the PI backbone is a consequence of the high percentage of PMMA, which is in agreement with the observed increase in the Young's Modulus of both grafted materials when compared to the one of PI. The difference between the

Table 1
Young's modulus, stress at break and tensile toughness of PI, PI-*g*-PMMA and PI-*g*-PMMA/NPs.

	Young's modulus (GPa)	Stress at break (MPa)	Elastoplastic energy per unit volume (J m^{-3})	Strain at break (%)
PI	$(1.5 \pm 0.3)10^{-4}$	–	–	–
PMMA	1.8 ± 0.1	27 ± 2	$(3.4 \pm 0.6)10^5$	2.4 ± 0.1
PI-*g*-PMMA	1.2 ± 0.1	21 ± 2	$(10.4 \pm 1.5)10^5$	6.0 ± 0.1
PI-*g*-PMMA/NPs	1.8 ± 0.1	33 ± 3	$(6.0 \pm 1.0)10^5$	3.0 ± 0.1

Table 2
Wear coefficients of PMMA, PI-*g*-PMMA and PI-*g*-PMMA/NPs.

	Wear coefficient (mm^3/mN)
PMMA	$(5.7 \pm 0.6)10^{-6}$
PI-*g*-PMMA	$(1.2 \pm 0.3)10^{-6}$
PI-*g*-PMMA/NPs	$(1.9 \pm 0.2)10^{-6}$

Young's Modulus of PI-*g*-PMMA and the one of PI-*g*-PMMA/NPs, may be attributed to the $BaSO_4$ nanoparticles as their Bulk Modulus (63 ± 2 GPa [33]) increases the Young's Modulus of the composite.

3.5. Ball cratering micro-scale wear test

The calculated values for the wear coefficient are reported in Table 2. A recent review suggest that the wear coefficient of a given material is strongly related to its ability to absorb the energy involved in abrasion processes and transform it into plastic deformation [34]. In this sense, PI-*g*-PMMA should have the higher wear resistance, i.e. the lowest wear coefficient. The obtained results are in agreement with this hypothesis and also demonstrate that brittle materials have low wear resistance, as can be seen in the value obtained for PMMA. In the case of PI-*g*-PMMA/NPs, the composite material shows a fragile behaviour. However, its wear coefficient is more similar to the one measured in PI-*g*-PMMA as a consequence of the tensile toughness of the polymeric matrix (PI-*g*-PMMA). This result may be understood taking into consideration that the fragility of the materials was evaluated through tensile tests, which is the most unfavourable condition for a nanoparticle reinforced material. On the contrary, when the material is tested under compression the influence of weak interface linkage between the polymer matrix and the nanoparticles is less noticeable. In the ball cratering micro-scale wear test the material is tested under compression and shear stress. The tensile toughness of the polymer matrix (PI-*g*-PMMA) of the composite may lead to an enhancement in its wear resistance compared to PMMA.

In summary, a new composite material (PI-*g*-PMMA/NPs) capable of retaining $BaSO_4$ nanoparticles homogeneously distributed within the polymer matrix was developed. This may be explained by the electrostatic interactions between the $BaSO_4$ and the carboxylate functional groups of the methacrylate units. This new material, whose polymeric matrix can absorb more elastoplastic energy during deformation than PMMA, can withstand higher stress at break and strain at break than this commercial polymer (22% and 25% respectively). In this sense, it could be a suitable replacement for PMMA in acrylic bone cement formulations.

Additionally, PI-*g*-PMMA/NPs presents an enhancement in its wear resistance when compared to commercial PMMA (a 66% decrease in its wear coefficient). The combination of the results reported in this paper suggests that the structure of the developed material may be represented by the scheme shown in Fig. 10.

4. Conclusions

A new material having potential applications in vertebroplasty and kyphoplasty was developed. This polymeric matrix is tougher than the traditional PMMA matrix usually employed in these surgical treatments. It has also the ability to confine the contrast agent nanoparticles thus avoiding or diminishing their agglomeration. This new material is a graft polymer having PI backbone and PMMA branches, where the confinement and homogenous distribution of the $BaSO_4$ nanoparticles is attributed their interaction with the PMMA side chains. Additionally, these PMMA branches allow its compatibilization with PMMA homopolymer matrix.

From the analysis of the RMN spectrum and the proposed grafting reaction mechanism it is possible to conclude that it is highly probable that each and every isoprene unit is grafted with short PMMA side chains (3.75 MMA units on average), having low dispersion in the length of these side chains.

The mechanical behaviour of the grafted materials with and without nanoparticles indicate the rigidization of the PI backbone due to the anchoring of PMMA as there is a considerable increase in the Young's Modulus compared to PI. Additionally, both tensile toughness (elastoplastic energy per unit volume until fracture) and wear resistance of the grafted materials are higher to those corresponding to commercial PMMA, which is mainly a fragile material.

The addition of $BaSO_4$ nanoparticles has no significant effect on the T_g, as no difference is observed between PI-*g*-PMMA/NPs and PI-*g*-PMMA, the polymeric matrix. However, these T_gs are higher than the one observed in PI due to the presence of more rigid side chains (PMMA).

The addition of $BaSO_4$ nanoparticles increases both stress at break and Young's modulus when compared to the polymeric matrix. However, the strain at break and wear resistance are negatively affected because of the existence of weak linking zones between the nanoparticles and the polymer matrix.

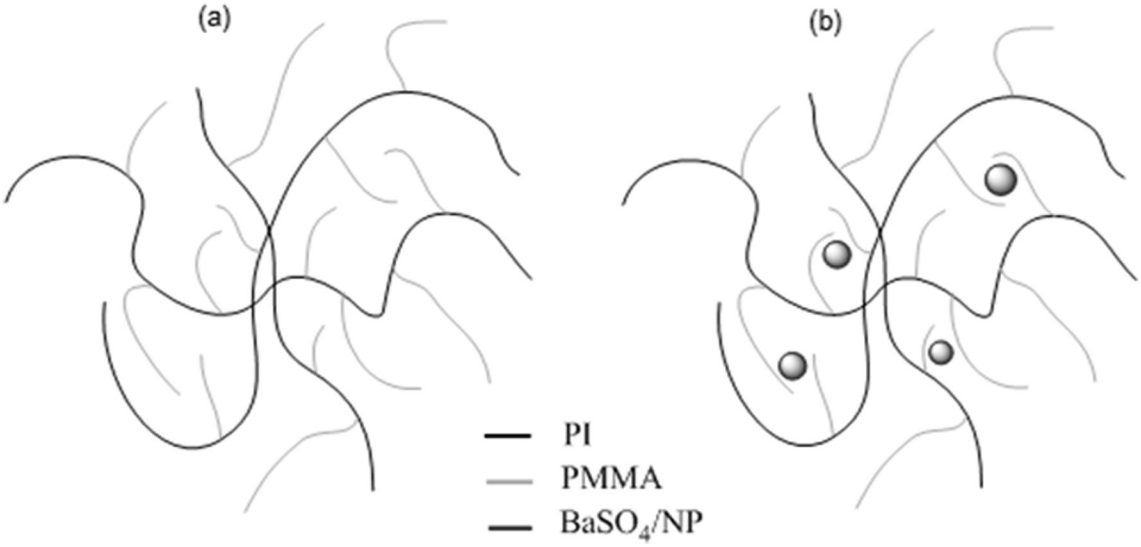

Fig. 10. Branching schemes of (a) PMMA-*g*-PI and (b) PMMA-*g*-PI/NPs.

This new composite material has the potential of improving acrylic bone cement toughness when using it to replace part of the PMMA homopolymer. Finally, the homogeneous distribution of the contrast agent among the polymeric matrix may help reducing the amount of BaSO4 needed to achieve a desirable fluoroscopic control.

Notes

The authors declare no competing financial interest.

Acknowledgements

The authors thank the financial support of UBACyT (No. 20020130100495BA and 20020130100021BA), ANPCyT (PICT-2012-0717 and PICT-2012-1093), and CONICET (PIP 2013-2015, 11220120100508CO and 11220110100370CO) and the fellowship of M.H. L.

Appendix A. Supplementary data

Supplementary data to this article can be found online at http://dx.doi.org/10.1016/j.msec.2015.10.097.

References

[1] M.H. Lissarrague, M.L. Fascio, S. Goyanes, N.B. D'Accorso, Acrylic bone cements: the role of nanotechnology in improving osteointegration and tunable mechanical properties, J. Biomed. Nanotechnol. 10 (2014) 3536–3557.
[2] B. Magnan, M. Bondi, T. Maluta, E. Samaila, L. Schirru, C. Dall'Oca, Acrylic bone cement: current concept review, Musculoskelet. Surg. 97 (2013) 93–100.
[3] J. Graham, C. Ahn, N. Hai, Effect of bone density on vertebral strength and stiffness after percutaneous vertebroplasty, Spine 32 (2007) E505–E511.
[4] S.G. Pneumaticos, G.K. Triantafyllopoulos, D.S. Evangelopoulos, J.A. Hipp, M.H. Heggeness, Effect of vertebroplasty on the compressive strength of vertebral bodies, Spine J. 13 (2013) 1921–1927.
[5] R. Gillani, B. Ercan, A. Quiao, T.J. Webster, Nanofunctionalized zirconia and barium sulfate particles as bone cement additives, Int. J. Nanomedicine 5 (2010) 1–11.
[6] J.G.F.J. Santos, V.J.R.R. Pita, P.A. Melo, M. Nele, J.C. Pinto, Production of bone cement composites: effect of fillers, co-monomer and particles properties, Braz. J. Chem. Eng. 28 (2011) 229–241.
[7] M. Arora, E.K.S. Chan, S. Gupta, A.D. Diwan, Polymethylmethacrylate bone cements and additives: a review of the literature, World J. Orthop. 4 (2013) 67–74.
[8] D.C. Rodrigues, R.A. Bader, J.M. Hasenwinkel, Grafting of nanospherical PMMA brushes on cross-linked PMMA nanospheres for addition in two-solution bone cements, Polymer 52 (2011) 2505–2513.
[9] S.B. Neoh, A.S. Hashim, Highly grafted polystyrene-modified natural rubber as toughener for polystyrene, J. Appl. Polym. Sci. 93 (2004) 1660–1665.
[10] S. Chuayjuljit, S. Moolsin, P. Potiyaraj, Use of natural rubber-g-polystyrene as a compatibilizer in casting natural rubber/polystyrene blend films, J. Appl. Polym. Sci. 95 (2005) 826–831.
[11] A.-D.N. Celestine, B.A. Beiermann, P.A. May, J.S. Moore, N.R. Sottos, S.R. White, Fracture-induced activation in mechanophore-linked, rubber toughened PMMA, Polymer 55 (2014) 4164–4171.
[12] D. Quan, A. Ivankovic, Effect of core–shell rubber (CSR) Nano-particles on mechanical properties and fracture toughness of an epoxy polymer, Polymer 66 (2015) 16–28.
[13] A. Bhattacharya, B.N. Misra, Grafting: a versatile technique to modify polymers. Techniques, factors and applications, *prog*, Policy. Sci. 29 (2004) 767–814.
[14] D. Cangialosi, C. Lindsay, P.T. Mc Grail, G. Spadaro, Study of methyl methacrylate polymerization in the presence of rubbers, Eur. Polym. J. 37 (2001) 535–537.
[15] E. Kalkornsurapranee, K. Sahakaro, A. Kaesamann, C. Nakason, From a laboratory to a pilot scale production of natural rubber grafted with PMMA, J. Appl. Polym. Sci. 114 (2009) 587–597.
[16] L. Vayachuta, P. Phinyocheep, D. Derouet, S. Pascual, Synthesis of NR-g- PMMA by "grafting from" method using ATRP process, J. Appl. Polym. Sci. 121 (2011) 508–520.
[17] D. Derouet, Q.N. Tran, J.L. Leblanc, Physical and mechanical properties of poly(methyl methacrylate)-grafted natural rubber synthesized by methyl methacrylate photopolymerization initiated by N,N-diethyldithiocarbamate functions previously created on natural rubber chains, J. Appl. Polym. Sci. 112 (2009) 788–799.
[18] O. Azzaroni, O. Polymer Brushes, Here, there and everywhere: recent advances in their practical applications and emerging opportunities in multiple research fields, *J. Polym. Sci. Part A*, Polym. Chem. 50 (2012) 3225–3258.
[19] A. Ahmad, M.Y.A. Rahman, M. Su'ait, H. Hamzah, Study of MG49-PMMA based solid polymer electrolyte, Open Mater. Sci. J. 11 (2011) 170–177.
[20] A. Ahmad, M.Y.A. Rahman, H. Harun, M.S. Su'ait, M.A. Yarmo, Preparation and characterization of 49% poly(methyl methacrylate) grafted natural rubber (MG49) – stannum (IV) oxide (SnO2) – lithium salt based composite polymer electrolyte, Int. J. Electrochem. Sci. 7 (2012) 8309–8325.
[21] A. Sargsyan, A. Tonoyan, S. Davtyan, C. Shick, The amount of immobilized polymer in PMMA SiO2 nanocomposites determined from calorimetric data, Eur. Polym. J. 43 (2007) 3113–3127.
[22] A. Kassman, S. Jacobson, L. Erickson, P. Hedenqvist, M.A. Olsson, New method for the intrinsic abrasion resistance of thin coatings, Surf. Coat. Technol. 50 (1991) 74–85.
[23] H. Sato, Y. Tanaka, ^{1}H-NMR study of polyisoprenes, J. Polym. Sci. Part A Polym. Chem. 17 (1979) 3551–3558.
[24] T. Kochthongrasamee, P. Prasassarakich, S. Kiatkamjornwong, Effects of redox initiator on graft copolymerization of methyl methacrylate onto natural rubber, J. Appl. Polym. Sci. 101 (2006) 2587–2601.
[25] D.L. Hall-Edgefield, T. Shi, K. Nguyen, A. Sidorenko, Hybrid molecular brushes with chitosan backbone: facile synthesis and surface grafting, Appl. Mater. Interfaces 6 (2014) 22026–22033.
[26] H. Garate, I. Mondragon, S. Goyanes, N.B. D'Accorso, Controlled epoxidation of poly(-styrene-*b*-isoprene-*b*-styrene) block copolymer for the development of nanostructured epoxy thermosets, J. Polym. Sci. Part A Polym. Chem. 49 (2011) 4505–4515.
[27] H. Bala, W. Fu, J. Zhao, X. Ding, Y. Jiang, K. Yu, Z. Wang, Preparation of $BaSO_4$ nanoparticles with self-dispersing properties, Colloids Surf. A Physicochem. Eng. Asp. 2052 (2005) 129–134.
[28] M. El-Shahate, I. Saraya, I.M. Bakr, Synthesis of $BaSO_4$ nanoparticles by precipitation using polycarboxylate as modifier, Am. J. Nanotechnol. 2 (2011) 106–111.
[29] L.E. Manring, Thermal degradation of poly(methy1 methacrylate). 2. Vinyl-terminated polymer, Macromolecules 22 (1989) 2673–2677.
[30] L.E. Manring, Thermal degradation of poly(methy1 methacrylate). 4. Random side-group scission, Macromolecules 24 (1991) 3304–3309.
[31] H. Oh, P.F. Green, Polymer chain dynamics and glass transition in athermal polymer/nanoparticle mixtures, Nat. Mater. 8 (2009) 139–143.
[32] L.M. Famá, V. Pettarin, S.N. Goyanes, C.R. Bernal, Starch/multi-walled carbon nanotubes composites with improved mechanical properties, Carbohydr. Polym. 83 (2011) 1226–1231.
[33] P.-L. Lee, E. Huang, S.C. Yu, High pressure raman and X-ray studies of barite, $BaSO_4$, High Pressure Res. 23 (2003) 439–450.
[34] T.V. Duncan, Release of engineered nanomaterials from polymer nanocomposites: the effect of matrix degradation, Appl. Mater. Interfaces 7 (2015) 20–39.